Available online at www.sciencedirect.com

ScienceDirect

Structural Integrity Procedia 00 (2021) 000–000

Structural Integrity Procedia

www.elsevier.com/locate/procedia

FATIGUE DESIGN 2021, 9th Edition of the International Conference on Fatigue Design

Effects of Powder Particle Size on Fatigue Performance of Laser Powder-Bed Fused Ti-6Al-4V

Arash Soltani-Tehrani[a,b], Mohammad Salman Yasin[a,b], Shuai Shao[a,b], Meysam Haghshenas[c], Nima Shamsaei[a,b,*]

[a]*Department of Mechanical Engineering, Auburn University, Auburn, AL 36849, USA*
[b]*National Center for Additive Manufacturing Excellence (NCAME), Auburn University, AL 36849, USA*
[c]*Department of Mechanical, Industrial, and Manufacturing Engineering, University of Toledo, Toledo, OH 43606, USA*

Abstract

In powder-based metal additive manufacturing, one key specification that needs to be precisely optimized is the particle shape and size distribution of metallic powders. Particle shape and size distribution influences the flowability of the powder and the uniformity of powder bed density (i.e. packing state of the powder). These eventually affect the porosity, which ultimately influences the fatigue performance of the fabricated parts. Therefore, it is essential to understand the effect of powder characteristics on the fatigue behavior before additively manufactured parts can be used in load-bearing, safety-critical applications. The current study aims at assessing the effects of powder particle size and morphology on mechanical properties and fatigue response of laser beam powder bed fused (LB-PBF) Ti-6Al-4V; an alpha-beta workhorse alloy of the titanium family. Several Ti-6Al-4V powder batches with different size distributions are used to fabricate the parts employing an EOS M290 machine. Powder characteristics, including flowability, compressibility, cohesion, size, and shape morphology, are investigated to reveal the differences between the two tested powder batches. Porosity levels and mechanical testing results are compared among specimens fabricated from different powder batches and the differences are explained based on variations in powder characteristics.

Keywords: Additive manufacturing; Laser beam powder bed fusion; Ti-6Al-4V; Fatigue; Particle size distribution; Powder flowability

* *Corresponding author. Tel: +1-334-844-4839*
E-mail address: shamsaei@auburn.edu

1. Introduction

Due to the thriving interest in laser beam powder bed fusion additive manufacturing (LB-PBF), understanding metallic powder, which is used as the feedstock material in the LB-PBF processes, has recently gained a lot of attention (Shamsaei et al., 2015). Granular powder, however, is typically complex as it can be consisted of solid (i.e., particles), gas (i.e., gas-entrapped pockets within the powder bulk), and liquid (i.e., in case of moisture absorption). In addition, powders have multiple characteristics including, but not limited to, particle size distribution (PSD), shape, surface chemistry, and microstructure which further entangles its interpretation (Carrion, Soltani-Tehrani, Phan, & Shamsaei, 2019; Soltani-Tehrani, Pegues, & Shamsaei, 2020).

Before the widespread adoption of AM technologies, it is important to assess how the powder characteristics are correlated with the part performance and more specifically fatigue resistance in load critical applications (Daniewicz & Shamsaei, 2017; Yadollahi & Shamsaei, 2017). In this study, the particle size distribution (PSD) of the powders will be specifically investigated. The PSD is reported as one of the main factors governing powder behavior including flowability and packing state (Sutton, Kriewall, Leu, & Newkirk, 2017; Tan, Wong, & Dalgarno, 2017). Recently, researchers have tried to shed light on the effects of PSD on the powder behavior and consequently the part performance of additive manufactured (AM) parts (Jian et al., 2021).

Nomenclature

AB	As-built
AE	Aeration energy
AM	Additive manufacturing
AM	Additive manufactured
AMSC	America Makes & ANSI Additive Manufacturing Standardization Collaborative (AMSC)
%EL	Percent elongation to failure
HCF	High-cycle-fatigue
HRC	Rockwell C hardness
LB-PBF	Laser beam powder bed fusion
LCF	Low-cycle-fatigue
M	Machined
MCF	Mid-cycle-fatigue
NHT	Non-heat-treated
PSD	Particle size distribution
Ti64	Ti-6Al-4V
UTS	Ultimate tensile strength
YS	Yield strength

Cordova et al. (2020) showed that the presence of spherical particles in powders can considerably increase their flowability. In addition, it was reported that finer particles can result in a superior packing state while coarser particles tend to increase the powder flowability. Therefore, the compensation between flowability and packing state can be a challenge in LB-PBF. It was also shown that powder bulk density is an important factor to govern powder flowability. For example, almost similar flowabilities were noted for the AlSi10Mg and Scalmalloy as they have almost identical bulk densities. Similar research on the LB-PBF Ti-6Al-4V (Ti64) part performance showed that less spherical powder particles are more sensitive to the manufacturing parameters such as layer thickness (Brika, Letenneur, Dion, & Brailovski, 2020). Additionally, it has been reported that the presence of fine particles can adversely affect the powder flowability and even the packing state in case of agglomeration due to higher inter-particle frictional forces of fine particles (German, 1984; Tan et al., 2017). In this study, the parts fabricated with the coarser PSD showed superior ultimate tensile strength (UTS) and slightly lower percent elongation to failure (%EL) or ductility as compared to the finer powder. Still, the parts fabricated with the coarser powder had higher part densities. Interestingly, the part

performance variations observed as a result of different PSDs in the literature can be dependent on the manufacturing system, i.e., LB-PBF or electron beam powder bed fusion (EB-PBF) as well as different material systems.

In this regard, Nandwana et al. (2018) investigated the effects of different PSDs on the performance of EB-PBF Ti64 parts. A higher UTS was noted for the coarser PSD in both horizontally- and vertically-fabricated specimens. On the other hand, the finer powder showed better high cycle fatigue (HCF) performance than the coarse batch. Opposite results have been reported for the LB-PBF AlSi10Mg by Jian et al. (2021). In this study, it was stated that the specimens manufactured from the coarser batch can have much higher ductility (~two times greater) and almost identical UTS values.

In terms of fatigue performance, it was observed the coarser batch has typically a higher HCF performance for different stress ratios (R) including -1, 0, and 0.5. The higher ductility and fatigue resistance of LB-PBF coarse AlSi10Mg specimens was correlated with the smaller and fewer number of defects in this batch. The critical defect size in the coarse powder specimens was almost half of the ones in the fine powder specimens. Conversely, Riener et al. (2020) observed negligible variations in tensile properties including UTS, yield strength (YS), and %EL of LB-PBF AlSi10Mg parts fabricated with different PSDs. However, higher surface roughness was noted for the specimens manufactured from the finer powder.

As it is vivid, the question of "how PSD can affect the mechanical performance of AM Parts?" has been remained unanswered, which necessitates a more careful examination of PSD variations. As a result, two Ti64 powders with different PSDs were used to evaluate the effects of particle size on the powder behavior. In addition, the mechanical performance of the parts was assessed by performing tensile and fatigue tests. Some discussions will be provided to correlate the observed variations in powder with the part performance. Lastly, some conclusions will be drawn based on the results. This article will further contribute to some major technical gaps associated with PSD and reported in America Makes & ANSI Additive Manufacturing Standardization Collaborative (AMSC) Roadmap (America Makes & AMSC, 2018).

2. Experimental Program

In this study, plasma-atomized Ti64 powders with PSDs of 15-53 µm (coarse) and 15-45 µm (fine) were used. Both powders had an almost comparable concentration of alloying elements. The same layout was fabricated with both powders using LB-PBF EOS M290 machine, by employing a 280-W laser power, 1200-mm/s scanning speed, 0.14-mm hatching distance, and 30-µm layer thickness. In addition, argon was used as the shielding gas during fabrication. As seen in Fig.1, the build plates consisted of net-shaped fatigue specimens according to ASTM E466 which were later tested in as-built (AB) surface condition, and cylindrical rods which were machined to geometries of fatigue and tensile specimens according to ASTM E466 and ASTM E8, respectively (ASTM International, 2015, 2016), and tested in their machined (M) surface condition.

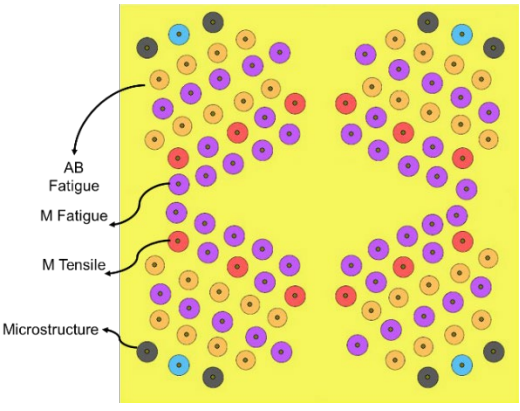

Fig. 1. The top view of the build layout used for fabrication of LB-PBF Ti64 parts.

After fabrication, parts were detached from the build plate, and some parts were selected for heat treatment. The heat treatment was consisted of stress relief (SR) at 900 °C for one hour and cooled to room temperature inside the furnace. After SR, the cylindrical rods were machined into the geometry of fatigue and tensile test specimens as illustrated in Fig 2. Additionally, specimens for microstructural characterizations were cut along the longitudinal plane and they were etched using the modified Kroll's reagent (10% HF: 10% HNO_3:80% distilled water) to reveal the microstructure as well as the melt pool boundaries.

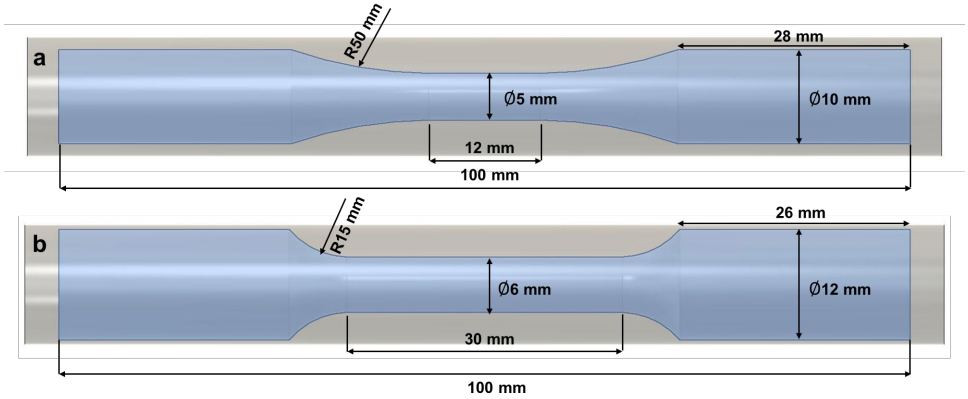

Fig. 2 Net-shaped geometry of (a) fatigue specimens according to ASTM E466 (ASTM International, 2015) and (b) tensile according to the ASTM E8 (ASTM International, 2016).

Some specimens from both powder batches were selected for X-ray-CT. The X-ray-CT was conducted with a voxel size of 6 µm. However, defects smaller than 10 µm were excluded from analyses. Tensile tests were conducted in displacement-control with an equivalent strain rate of 0.001 mm/mm.s^{-1}. All tensile tests were paused at 0.05 mm/mm (5%) strain to remove the extensometer and then continued until the final fracture. The UTS, YS, and %EL were also measured. For fatigue, tests were performed in force-control mode and the cyclic stress rate was kept constant for all the specimens. Fatigue tests were conducted at different stress amplitude levels and the tests which reached 5×10^6 cycles (i.e., 10^7 reversals) were considered as run-out or no failure test.

In addition, hardness tests were performed using a LECO LCR 500 with a 60 µN/s load rate. Rockwell C (HRC) was used to indent and report the results as recommended by the manufacturer for Ti64. Powder characteristics including compressibility and cohesion were investigated by a Freeman Technology (FT4) powder rheometer. Followed by the experimental program, experimental results will be provided and discussed. Any variation observed in part performance will be correlated with the powder characteristics. Lastly, some conclusions will be made based on the results.

3. Experimental Results and Discussion

At first, compressibility was evaluated which is representative of the powder packing state. The compressibility can indicate how the powder density changes when normal stress is applied (Brika et al., 2020; Freeman Technology, 2008). Therefore, a powder with lower compressibility is desired for the LB-PBF representing fewer empty spaces (voids) among the particles. These voids are entrapped within the solidified material resulting in the formation of volumetric defects, and specifically, gas-entrapped pores. As seen in Fig. 3, coarse powders possess higher compressibility compared with fine powders. This means that the coarse powder requires more compaction to become fully dense. As a result, it can be postulated that fine powders possess a better particle arrangement with fewer empty spaces within the powder bulk, while more defects can be expected in the specimens manufactured from the coarse powders.

Another factor that was investigated in the present study is cohesion. Cohesion is obtained as an output of the shear cell test with the FT4, and it shows the resistance of powder to shearing and flow. Therefore, a powder with lower

resistance and consequently cohesion is desired for LB-PBF due to its superior flowability.

The higher flowability would result in higher spreadability and a more uniform powder layer on the build plate. As seen in Fig. 4, almost identical flowabilities are observed with a slight inclination toward the fine powder. The marginally higher cohesion of fine powder can be well correlated with the span values. The span, defined as the D_{90}-D_{10}/D_{50}, where a D_x of y represents that x% of particles are smaller than y, can show the uniformity of powder particles. Powders with smaller spans are typically better-balanced in size and provide a higher flowability (Carrion et al., 2019; Soltani-Tehrani et al., 2020).

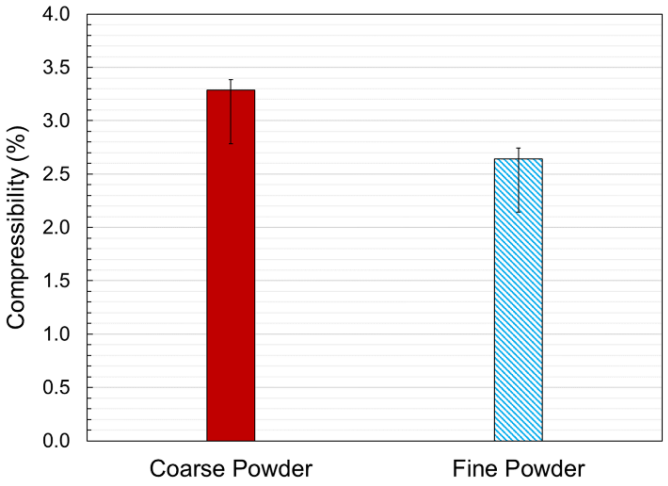

Fig. 3 Compressibility of the coarse and fine powders obtained by the FT4 powder rheometer.

The span of the fine powder was slightly narrower than the coarse one, illustrating a good correlation with the flow and packing behaviors. The identical flowabilities observed in both powder batches can be attributed to the presence of highly spherical powder particles with minimum porosity (Moghimian et al., 2021). This hypothesis is also echoed in the bulk densities which were 2.9 and 2.8 g/cm^3 for the coarse and fine powders, respectively.

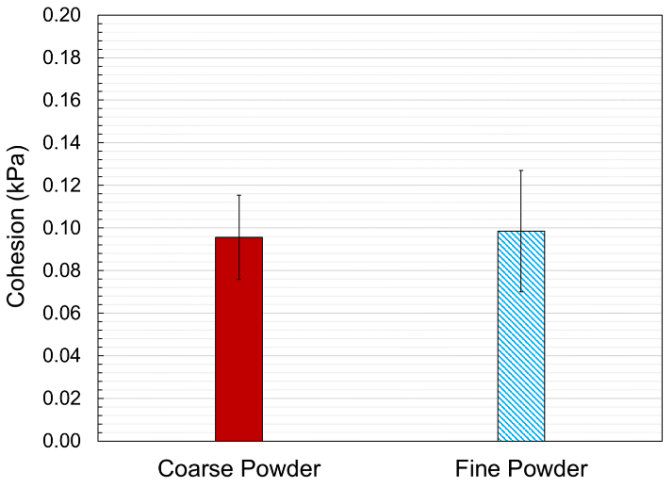

Fig. 4 Cohesion of the coarse and fine powders obtained by the FT4 powder rheometer.

Upon characterizing the powders, the microstructural assessment was performed to investigate whether different PSDs can alter the microstructure or not. As seen in Fig. 5, the microstructure of the coarse and fine powder specimens in the non-heat-treated (NHT) condition is illustrated. No clear difference was noted in the microstructure of the parts in the NHT condition due to different particle sizes. The microstructure consists of martensitic α in prior β columnar grains. The melt pool depth and overlap depth were measured according to the NASA MSCF 3717 as illustrated in Fig. 5(c). In this method, the melt pool depth, dp_n, and overlap depth, do_n, are evaluated from the top layer, and normalized with the layer thickness (i.e., 30 µm).

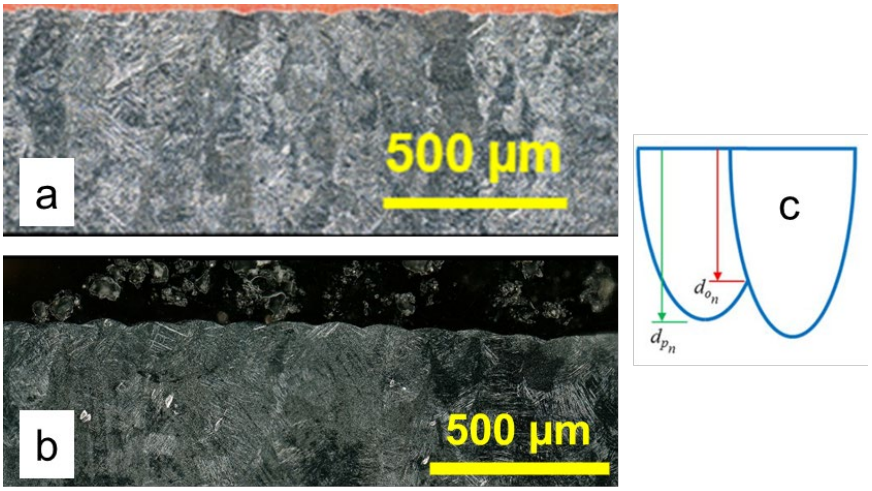

Fig. 5 Melt pool illustrations for the (a) coarse and (b) fine powder specimens as well as (c) the schematic of a melt pool depth and overlap depth adapted from NASA MSFC 3717 (NASA, 2017).

It was seen that the ratio of melt pool depth and overlap depth to layer thickness are 2.4 and 1.5, respectively in the case of coarse powder and 4.7 and 3.3 for fine powder specimens. Ratios larger than one indicates enough remelting between subsequent layers and the absence of a lack of fusion defects. The larger melt pool depths (i.e., larger laser penetration depth) in the fine powder specimens can be attributed to the higher absorptivity of finer particles (Spierings, Herres, & Levy, 2011). Therefore, larger particles require more input energy density resulting in higher cooling rates during fabrication and consequently shallower melt pools (Shrestha, Shamsaei, Seifi, & Phan, 2019; Soltani-Tehrani, Shrestha, Phan, Seifi, & Shamsaei, 2021). Similar results were noted in the HRC values. As seen in Fig. 6, the HRC results did not show much variation between the coarse and fine powder specimens in the NHT condition, which can be attributed to comparable microstructures resulted from different PSDs.

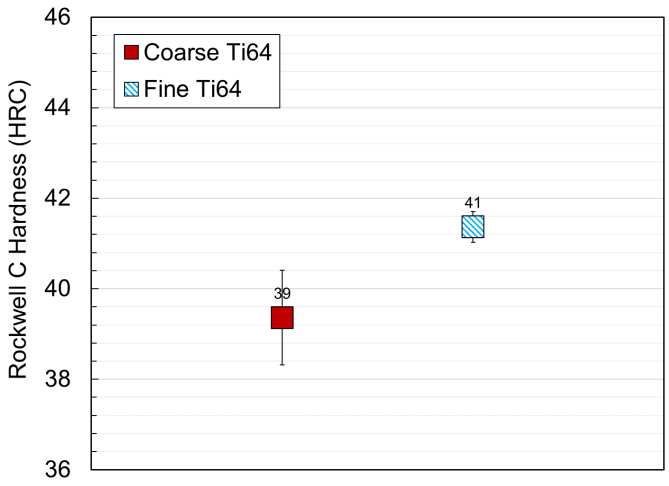

Fig. 6 HRC values for the coarse and fine Ti64 powder specimens.

Tensile tests performed on both sets revealed that the UTS is slightly higher for the fine powder, similar to the HRC results (see Fig. 7). Ductility, represented by the %EL, was remarkably higher for the case of coarse powder. Noting a higher ductility for coarse powder specimens is quite interesting as ductility is directly correlated with defect content. Previously, it was predicted that fine powder possesses a superior packing behavior whereas the coarse powder specimens showed a higher ductility.

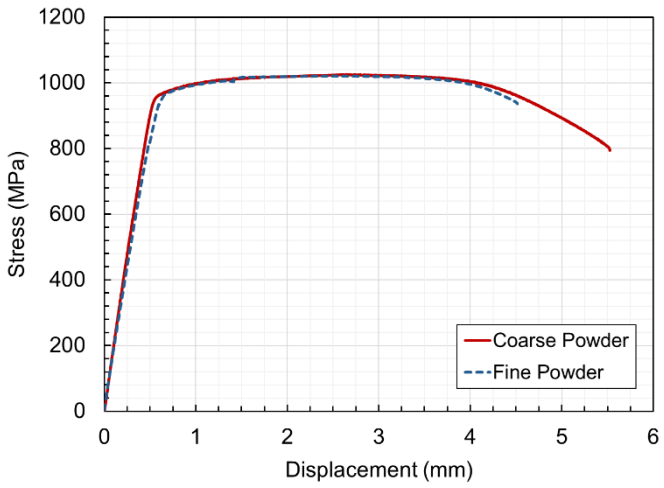

Fig. 7 Engineering stress-displacement curves for the coarse and fine powder specimens.

Although these observations were consistent with the results in Ref. (Jian et al., 2021), the defect content was evaluated to understand why the coarse powder specimens provide higher ductility. Upon investigation of the volumetric defects in the specimens manufactured from the coarse and fine powders, the coarse powder specimens had higher porosity as compared to the fine powder specimens (99.991% vs. 99.994%, respectively), as expected. The average defect size was also 32 μm for the coarse and 13 μm for the fine powder specimens, illustrating the less amount of porosity in the fine powder specimens.

Upon more careful observations with Xray-CT, some large defects were detected in the fine powder specimens.

For instance, a maximum defect size of 194 µm was found in the fine powder specimen whereas it was 102 µm in the counterpart manufactured from the coarse powder. The very large defects in the fine powder were hypothesized to be secondary phase particles, resulted from spattering during fabrication (Sutton, Kriewall, Leu, Newkirk, & Brown, 2020). Therefore, the lower ductility of fine powder specimens can be attributed to larger critical defect sizes due to the higher chance of spattering and/or thicker oxide films around the finer particles (i.e., more surface to volume ratio) (Leung et al., 2019).

Lastly, the fatigue performance was evaluated for the specimens in their machined surface condition. As seen in Fig. 8, the bar charts represent the low-, mid- and high-cycle fatigue (LCF, MCF, and HCF) regimes. It can be seen that the coarse powder specimens had superior fatigue performance in the LCF (i.e., 700 MPa) and MCF (i.e., 500 MPa). This behavior can be ascribed to the higher ductility of the coarse powder specimens, retarding the crack growth in these regimes. In the HCF (i.e., 400 MPa), although the difference was not significant, the coarse powder specimens still showed higher resistance to fatigue failures. In this regime, cracks always initiate from the near-to-surface or internal volumetric defects. It was noted the crack-initiating defects in the fine powder specimens are substantially larger than the ones in coarse powder. For instance, the critical defect size in a fine powder specimen was 110 µm whereas it was 64 µm in the counterpart specimen fabricated from the coarse powder. The observation on the superior fatigue performance of coarse powder specimens was also consistent with the results provided in Ref. (Jian et al., 2021).

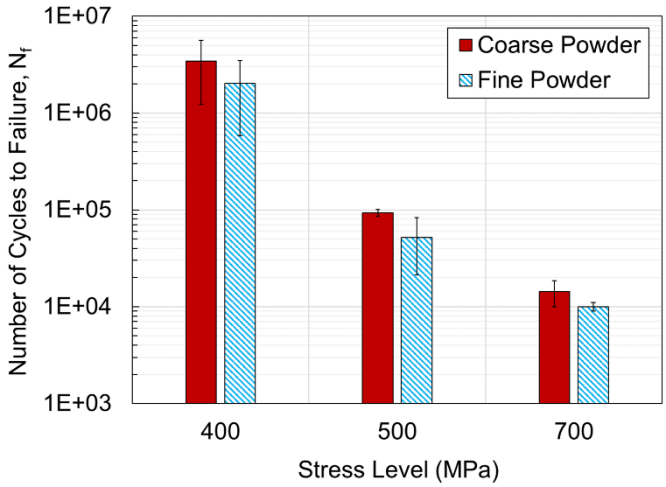

Fig. 8 Fatigue performance of the coarse and fine powder specimens at 400 MPa (HCF), 500 MPa (MCF), and 700 MPa (LCF) stress levels.

4. Conclusions

In this study, two sets of specimens were fabricated from Ti64 powders with different PSDs. Following conclusions were made based on the experimental results and observations:

- The fine powder showed a superior packing behavior which resulted in considerably fewer volumetric defects in the as-fabricated parts.
- Both coarse and fine powders showed comparable flowabilities owing to their highly spherical powder particles.
- Although fine powder specimens revealed fewer defects, the critical defect size was considerably larger in the specimens manufactured from this powder.
- Due to the presence of much larger defects in the fine powder specimens, an inferior ductility, as well as fatigue resistance, was noted for these specimens as compared with their counterparts fabricated from the coarse powder.

Acknowledgments

This material is based upon work partially supported by the National Institute of Standards and Technology (NIST) under grant # 70NANB17H295.

References

America Makes, & AMSC. (2018). Standardization Roadmap for Additive Manufacturing - Version 2.0. *America Makes & ANSI Additive Manufacturing Standardization Collaborative (AMSC)*, *2*(June), 1–203.

ASTM International. (2015). E466 Standard Practice for Conducting Force Controlled Constant Amplitude Axial Fatigue Tests of Metallic Materials. *West Conshohocken, PA; ASTM International*. https://doi.org/10.1520/E0466-15.2

ASTM International. (2016). E8/E8M Standard Test Methods for Tension Testing of Metallic Materials. *West Conshohocken, PA; ASTM International*. https://doi.org/https://doi.org/10.1520/E0008_E0008M-13

Brika, S. E., Letenneur, M., Dion, C. A., & Brailovski, V. (2020). Influence of particle morphology and size distribution on the powder flowability and laser powder bed fusion manufacturability of Ti-6Al-4V alloy. *Additive Manufacturing*, *31*(November 2019), 100929. https://doi.org/10.1016/j.addma.2019.100929

Carrion, P. E., Soltani-Tehrani, A., Phan, N., & Shamsaei, N. (2019). Powder Recycling Effects on the Tensile and Fatigue Behavior of Additively Manufactured Ti-6Al-4V Parts. *JOM*, *71*(3), 963–973. https://doi.org/10.1007/s11837-018-3248-7

Cordova, L., Bor, T., de Smit, M., Campos, M., & Tinga, T. (2020). Measuring the spreadability of pre-treated and moisturized powders for laser powder bed fusion. *Additive Manufacturing*, *32*(December 2019), 101082. https://doi.org/10.1016/j.addma.2020.101082

Daniewicz, S. R., & Shamsaei, N. (2017). An introduction to the fatigue and fracture behavior of additive manufactured parts. *International Journal of Fatigue*, (94), 167.

Freeman Technology. (2008). *FT4 Powder Rheometer - Summary of Methodologies*.

German, R. M. (1984). Powder metallurgy science. In *Metal Powder Industries Federation*. 105 College Rd. E, Princeton, N. J. 08540, U. S. A.

Jian, Z. M., Qian, G. A., Paolino, D. S., Tridello, A., Berto, F., & Hong, Y. S. (2021). Crack initiation behavior and fatigue performance up to very-high-cycle regime of AlSi10Mg fabricated by selective laser melting with two powder sizes. *International Journal of Fatigue*, *143*(October 2020), 106013. https://doi.org/10.1016/j.ijfatigue.2020.106013

Leung, C. L. A., Marussi, S., Towrie, M., Atwood, R. C., Withers, P. J., & Lee, P. D. (2019). The effect of powder oxidation on defect formation in laser additive manufacturing. *Acta Materialia*, *166*, 294–305. https://doi.org/10.1016/j.actamat.2018.12.027

Moghimian, P., Poirié, T., Habibnejad-Korayem, M., Zavala, J. A., Kroeger, J., Marion, F., & Larouche, F. (2021). Metal Powders in Additive Manufacturing: A Review on Reusability and Recyclability of Common Titanium, Nickel and Aluminum Alloys. *Additive Manufacturing*, 102017. https://doi.org/10.1016/j.addma.2021.102017

Nandwana, P., Kirka, M. M., Paquit, V. C., Yoder, S., & Dehoff, R. R. (2018). Correlations Between Powder Feedstock Quality, In Situ Porosity Detection, and Fatigue Behavior of Ti-6Al-4V Fabricated by Powder Bed Electron Beam Melting: A Step Towards Qualification. *Jom*, *70*(9), 1686–1691. https://doi.org/10.1007/s11837-018-3034-6

NASA. (2017). *MSFC-SPEC-3717 - Specification for Control and Qualification of Laser Powder Bed Fusion Metallurgical Processes*. 58. https://doi.org/MSFC-SPEC-3717

Riener, K., Albrecht, N., Ziegelmeier, S., Ramakrishnan, R., Haferkamp, L., Spierings, A. B., & Leichtfried, G. J. (2020). Influence of particle size distribution and morphology on the properties of the powder feedstock as well as of AlSi10Mg parts produced by laser powder bed fusion (LPBF). *Additive Manufacturing*, *34*(February), 101286. https://doi.org/10.1016/j.addma.2020.101286

Shamsaei, N., Yadollahi, A., Bian, L., & Thompson, S. M. (2015). An overview of Direct Laser Deposition for additive manufacturing; Part II: Mechanical behavior, process parameter optimization and control. *Additive Manufacturing*, *8*, 12–35. https://doi.org/10.1016/j.addma.2015.07.002

Shrestha, R., Shamsaei, N., Seifi, M., & Phan, N. (2019). An investigation into specimen property to part performance relationships for laser beam powder bed fusion additive manufacturing. *Additive Manufacturing*, *29*(June), 100807. https://doi.org/10.1016/j.addma.2019.100807

Soltani-Tehrani, A., Pegues, J., & Shamsaei, N. (2020). Fatigue behavior of additively manufactured 17-4 PH stainless steel: The effects of part location and powder re-use. *Additive Manufacturing*, *36*, 101398. https://doi.org/10.1016/j.addma.2020.101398

Soltani-Tehrani, A., Shrestha, R., Phan, N., Seifi, M., & Shamsaei, N. (2021). Establishing Specimen Property to Part Performance Relationships for Laser Beam Powder Bed Fusion Additive Manufacturing. *International Journal of Fatigue*, 106384.

https://doi.org/10.1016/j.ijfatigue.2021.106384

Spierings, A. B., Herres, N., & Levy, G. (2011). Influence of the particle size distribution on surface quality and mechanical properties in AM steel parts. *Rapid Prototyping Journal*, *17*(3), 195–202. https://doi.org/10.1108/13552541111124770

Sutton, A. T., Kriewall, C. S., Leu, M. C., & Newkirk, J. W. (2017). Powder characterisation techniques and effects of powder characteristics on part properties in powder-bed fusion processes. *Virtual and Physical Prototyping*, *12*(1), 3–29. https://doi.org/10.1080/17452759.2016.1250605

Sutton, A. T., Kriewall, C. S., Leu, M. C., Newkirk, J. W., & Brown, B. (2020). Characterization of laser spatter and condensate generated during the selective laser melting of 304L stainless steel powder. *Additive Manufacturing*, *31*(October 2019), 100904. https://doi.org/10.1016/j.addma.2019.100904

Tan, J. H., Wong, W. L. E., & Dalgarno, K. W. (2017). An overview of powder granulometry on feedstock and part performance in the selective laser melting process. *Additive Manufacturing*, *18*, 228–255. https://doi.org/10.1016/j.addma.2017.10.011

Yadollahi, A., & Shamsaei, N. (2017). Additive manufacturing of fatigue resistant materials: Challenges and opportunities. *International Journal of Fatigue*, *98*, 14–31. https://doi.org/10.1016/j.ijfatigue.2017.01.001